Diamond & Related Materials 22 (2012) 96–104

Contents lists available at SciVerse ScienceDirect

Diamond & Related Materials

journal homepage: www.elsevier.com/locate/diamond

Cellular uptake and phototoxicity of surface-modified fluorescent nanodiamonds

Mao-Feng Weng [a,b], Bo-Jui Chang [a], Su-Yu Chiang [a,*], Niann-Shiah Wang [b], Huan Niu [c]

[a] National Synchrotron Radiation Research Center, Hsinchu 30076, Taiwan
[b] Department of Applied Chemistry, National Chiao Tung University, Hsinchu 30010, Taiwan
[c] Nuclear Science and Technology Department Center, National Tsing Hua University, Hsinchu 30013, Taiwan

ARTICLE INFO

Article history:
Received 24 December 2010
Received in revised form 16 August 2011
Accepted 22 December 2011
Available online 28 December 2011

Keywords:
Fluorescent nanodiamonds
Receptor-mediated endocytosis
Phototoxicity
Flow cytometry

ABSTRACT

Bioconjugated fluorescent nanodiamonds (FNDs) show potential for effectively targeted imaging and the enhanced photokilling of cancer cells. In this study, we investigated the mechanisms involved in the cellular uptake of surface-modified 140 nm FNDs and evaluated their cytotoxicity and phototoxicity following particle internalization. Through an analysis of flow cytometry, the internalized FND-Tf and FND-NH_2 particles reached their respective saturation values, with half-life times of approximately 0.8 h and 1.4 h. The determination indicated that the receptor-mediated endocytosis of FND-Tf particles was highly effective and nearly twice as efficient as the endocytic process of FND-NH_2 particles mainly through surface electrostatic interactions. The cytotoxicity of internalized particles was evaluated using the MTT assay, indicating that at saturation concentrations, the rate of proliferation of FND-treated cells decreases to less than half that of untreated cells. An examination of the phototoxicity of internalized FND-Tf particles under irradiation using a 532 nm laser revealed that the FND-treated cells could be killed using less than half the energy required for untreated cells. The enhanced cellular killing was attributed to FND particles converting light to thermal energy, with the support of Raman spectra of nanodiamond clusters that showed an increase in particle temperature under irradiation. Our results demonstrated that bioconjugated FNDs could be highly effective in the targeting of cancer cells for fluorescence imaging and photokilling with a minimum of collateral cell damage.

1. Introduction

Nanomaterials conjugated with biomolecules have been widely utilized in applications ranging from biology to medicine. These materials take advantages of their large surface to volume ratio to increase interactivity, and specific optoelectronic and magnetic properties to improve efficiency in cell targeting, imaging, and therapeutics [1–6]. Among them, fluorescent nanodiamonds (FNDs), a new type of carbon-based nanomaterial, are very attractive for biological applications due to their chemical and optical properties [7–22]. Several authors have demonstrated that FNDs have a low degree of cytotoxicity and a high degree of biocompatibility for various types of cells [10–14]. The facile formation of bioconjugated FNDs through electrostatic interactions and covalent bonding also promotes their use as drug delivery vehicles and cellular markers in diagnostics and therapeutics [15–17]. Applications to biological systems as targeted probes for long-term imaging and single-particle tracking *in vivo* have been reported; these applications take advantage of the excellent fluorescent properties of FNDs — protracted photostability without photobleaching and bright-red fluorescence [11–14].

The surface characteristics of surface charge and biologically active moieties that interact with cell membranes to transport particles along various endocytic pathways greatly influence the specificity and efficiency regarding cellular uptake [23–25]. Among the endocytic processes, the recognition of biologically active moieties is critically important as receptor-mediated endocytosis is a specific and effective pathway for the translocation of particles. Transferrin (Tf) of molecular weight approximately 80 kDa is a glycoprotein that targets preferentially transferrin receptor (TfR) to form a strongly bound complex. As transferrin receptors are commonly present on the surfaces of proliferating cells, Tf-conjugated nanoparticles are excellent candidates for the studies of receptor-mediated uptake and targeted drug/gene delivery [26–28]. In a previous study, we have demonstrated that 140 nm FNDs covalently conjugated with transferrins to form FND-Tf particles are capable of specifically targeting transferrin-receptors overexpressed on the surfaces of HeLa cells [15]. Following our work, Li and Zhou determined the half-life of this receptor-mediated endocytosis at 1.3 h [29]. However, a related study determined a half-life of 0.7 h for the receptor-mediated endocytosis of 140 nm FND conjugated with folic acid (FA) (abbreviated as FND-FA) [14]. The significant deviation in half-life between two receptor-mediated processes is unclear. In addition, the cellular uptake of positively charged particles can occur effectively through surface electrostatic interactions, but a comparison of the kinetics to the receptor-mediated uptake is rare. To study the electrostatic interactions, FND-NH_2 particles with amino groups on the

* Corresponding author.
E-mail address: schiang@nsrrc.org.tw (S.-Y. Chiang).

0925-9635/$ – see front matter © 2011 Elsevier B.V. All rights reserved.
doi:10.1016/j.diamond.2011.12.035

surface serve as a good model because amino group is a common functional group in biomolecules [30]. Hence, a kinetic study of cellular endocytosis using FND-Tf and FND-NH_2 particles should provide a better understanding of the mechanisms of the receptor-mediated processes and those through electrostatic interactions.

Bioconjugated gold-based and carbon-based nanomaterials have been shown to kill targeted cells effectively and selectively through photothermal effects attributed to their unique optical properties [31–44]. The absorption spectrum of FNDs shows a broad absorption of N-V° and N-V^- centers, with a maxima at ~570 nm and a bandwidth of ~100 nm, merging with the absorption of isolated nitrogen atoms with an onset at ~550 nm, according to that of a proton-irradiated Ib single crystal diamond [45]. The absorption at ≥530 nm is sufficiently separated from the spectral region of 300–500 nm in which endogenous cellular absorption occurs [46] that the application of internalized FNDs as photo-active agents for mediating cell death is an attractive option. The killing of lung cancer cells has been demonstrated through the two-photon absorption of surface-functionalized nanodiamonds (NDs) on the surface of cells at 532 nm; unfortunately, a number of dead control cells were also observed following comparable treatment due to the high quantities of energy associated with the laser [47]. To minimize the damage of untreated cells, the use of a low quantity of laser energy is essential for evaluating the phototoxicity of FNDs internalized by cells.

In this work, we investigated the uptake of FND-Tf and FND-NH_2 particles on HeLa cells as well as the cytotoxicity and phototoxicity of internalized particles to understand the effects of surface characteristics on cellular uptake and the potential of FNDs as photo-active agents. The quantity of internalized FND-Tf and FND-NH_2 particles as a function of particle concentration and reaction time was determined through an analysis of flow cytometry. Accordingly, we compared the effects of surface charge and biologically active moieties on the mechanisms of cellular uptake. To evaluate the cytotoxicity of internalized particles, the decrease in the rate of proliferation of cells following 24 h incubation at saturation particle concentrations was determined using the MTT assay. An examination of the phototoxicity of internalized FND-Tf particles was then performed under irradiation using a 532 nm laser. The enhancement in the killing of cells is attributed to the conversion of light absorbed by FND particles to heat, with the support of Raman spectra of nanodiamond clusters.

2. Experimental section

We prepared FND-COOH particles of ~140 nm and then functionalized their surfaces to form two FND variants — FND-Tf and FND-NH_2 for flow cytometry measurements and phototoxicity examination. Type Ib nanodiamond powders were obtained from Element Six. They were suspended in water at a concentration of 10 mg mL^{-1} and then deposited on a silicon wafer to form a nanodiamond film. The dried film was irradiated with a 2.5-MeV proton beam (KN, High Voltage, located in National Tsing Hua University in Taiwan) at a dose ~10^{16} ions cm^{-2} and then thermally annealed sequentially in vacuum at 800 °C for 4 h and in air at 600 °C for 2 h to form the nitrogen-vacancy (N-V) centers required for emission. To form FND-COOH, we treated the prepared FNDs with a mixture of concentrated H_2SO_4 and HNO_3 (volume ratio ~9) at 25 °C for 24 h, and then in a NaOH aqueous solution (0.1 M) at 90 °C for 2 h, and finally in an HCl aqueous solution (0.1 M) at 90 °C for 2 h, as described previously [15,48]. The formation of FND-Tf particles was performed by reacting transferrins (MW ~80 kDa, 0.1 mg) and FND-COOH (0.2 mg) in phosphate buffer saline (PBS, 1 mL, pH = 7.4) at 25 °C for 24 h, with the addition of N-(3-dimethylaminopropyl)-N′-ethyl-carbodiimide hydrochloride (5 mg) to activate the reaction. The FND-Tf particles were purified through a cycle involving separation by sedimentation using a centrifuge with suspension in PBS buffer, three times prior to use. FND-NH_2 particles were produced by adding FND-COOH (0.2 mg) particles to the 3-aminopropyltriethoxysilane (APTES) aqueous solution (1%) at 25 °C for 30 min and undergoing separation through centrifugation [16,49–51]. The use of APTES molecules is a well-known silanisation technique that involves the reaction between APTES molecules and residual hydroxyl group on the surface of FND-COOH, and subsequent condensation reactions to form an amino-silane film on the surface of FND-COOH.

The size distribution and zeta potential of FND-COOH, FND-NH_2, and FND-Tf particles were measured by suspending particles in deionized water at a concentration of 10 μg mL^{-1} with a particle analyzer (Delsa Nano C, Beckman-Coulter). To determine the cellular uptake, HeLa cells were cultured in DMEM (11965, Gibco) supplemented with fetal bovine serum (FBS, 10%) and penicillin/streptomycin (1%) at 37 °C in an incubator containing a humidified atmosphere of 5% CO_2. In each experiment, ~5×10^5 cells were seeded on a 12-mm round cover glass for 12 h before adding FND variants at 10 μg mL^{-1} to the medium for incubation. Differential contrast and fluorescence images of cells were acquired using a fluorescence microscope (TE2000, Nikon) with a mercury lamp for illumination. The treated cells were washed with PBS buffer three times to remove unbounded FND variants from the surface, whereupon it was fixed with 4% paraformaldehyde, and stained (Hoechst 33342) on the nuclei for fluorescence measurements. The fluorescent signals of FNDs and stained nuclei were collected at wavelengths of ≥590 and 460–500 nm, respectively. The quantity of internalized particles and reaction times were measured using flow cytometer (FACS Array, BD), equipped with a 532-nm laser for excitation and detection of fluorescence at wavelengths >685 nm.

For cellular growth inhibition assay, ~5×10^4 cells were seeded in medium in each of a 12-well plate (Becton Dickinson) for 12 h before adding FND variants at 0.1, 1, 10 or 20 μg mL^{-1}. Wide-field images of cells after incubation at 37 °C for 0, 24, 48 and 72 h were acquired using a 10× objective to examine cellular proliferation. The number of cells was counted with a counter; and MTT assay was performed with an Elisa reader (EMax, Molecular Devices) after treating cells with a MTT (3-(4,5-dimethylthiazol-2-yl)-2,5-diphenyltetrazolium bromide) testing solution at 37 °C for 4 h.

Phototoxicity assay was performed following exposure to a 100-W Hg lamp at selected wavelengths of 590–650 and 510–560 nm, or a continuous-wave (CW) laser at 532 nm (Millennia Vs, Spectra Physics). ~5×10^4 cells were seeded in the medium in each of an 8-well chambered cover glass (Lab-Tek™) at 37 °C overnight before 6 h incubation with FND-Tf particles at 1 or 10 μg mL^{-1}. The irradiation was focused through an objective (40× for Hg lamp and 20× for laser; both having N.A. = 0.75, Nikon) and wide-field images of cells were acquired using the same objective before and after irradiation for monitoring cell morphology. To confirm cell viability, cells were stained with calcein AM and ethidium homodimer-1 (EthD-1); the green fluorescence from calcein AM and the red fluorescence from EthD-1 indicate live and dead cells, respectively [32]. The Raman spectra of a nanodiamond cluster under 532 nm irradiation were measured using a spectrometer (iHR320, Jobin-Yvon) equipped with a CCD (DU940N-UVB, Andor) detector. A 60× water immersion objective (N.A. = 1.2, Nikon) was used to focus the irradiation on the sample and collect Raman signals before feeding them into the spectrometer.

3. Results and discussions

3.1. Cellular uptakes of FND variants

FND variants were prepared in three forms — FND-COOH, FND-NH_2 and FND-Tf for cellular uptake. FND-NH_2 particles were produced through cross links of APTES molecules to have amino groups on the outer surface of FND-COOH whereas FND-Tf bioconjugates were produced via the formation of an amide bond between FND-COOH and transferrin. The FNDs emit fluorescence in the region

Table 1
Measured size of particles and zeta potentials of FND variants.

Particles	Size (nm)	Zeta potential (mV)
FND-COOH	144 ± 8	−48.3 ± 1.3
FND-NH_2	166 ± 9	−25.4 ± 0.9
FND-Tf	222 ± 12	−51.6 ± 0.9

550–800 nm upon excitation at 532 nm. According to previous reports, the fluorescence is surface independent because the emission centers of FND are embedded in the crystal lattice [15,52]. Table 1 lists the sizes and charges of the particles determined by the DLS and zeta-potential, respectively. The surface thickness of FND-NH_2 is ~10–11 nm, estimated according to the difference in size between FND-NH_2 and FND-COOH. Similarly, the size of 222 nm for FND-Tf indicates a surface thickness of ~40 nm for transferrins immobilized on the surface of FND-COOH. The zeta potential of −51.6 mV for FND-Tf is consistent with the negative characteristics of free transferrins in solution. Despite an amino-silane film is formed on the outer surface of FND-COOH, the potential of FND-NH_2 is negative, −25.4 mV. This result suggests that not all the surface of FND-COOH is covered with amino groups. However, the influence of the carbonyl groups entirely covered by the film cannot be excluded. Vial et al. introduced hydroxyl groups homogeneously on the surface of ND-COOH by adsorption of octyl-β-D-glucopyranoside (OG) before the silanisation [50]. Despite the adsorption enabled a homogeneous coating of the amino-silane film on the surface of ND-COOH, they obtained a zeta potential of −27 mV for ND-NH_2, consistent with ours. Based on the results of various chemicals, Vial et al. concluded that the zeta potentials might not reflect solely the charges on the surface but also the hydration propensity; the experimental conditions might also govern the value and the sign of the zeta potential.

The uptake of FND-COOH, FND-NH_2, and FND-Tf particles by HeLa cells in DMEM with 10% FBS was monitored after 6 h incubation at a particle concentration of 10 μg mL^{-1}; one control experiment with FND-COOH particles in a medium without 10% FBS was performed for comparison. Fig. 1 shows epifluorescence images of internalized FND variants (left) and stained nuclei (middle), and their overlay with the differential interference contrast (DIC) image of cells (right); the internalization of FND variants was further confirmed from a series of vertical cross-sectional confocal fluorescence images of the treated HeLa cells. A comparison of Fig. 1(a)–(b) reveals negligible interaction of FND-COOH particles with cells in a serum-supplemented (10% FBS) medium; no FND-COOH image was observed in Fig. 1(a). The negative surface charges of FND-COOH particles prevented them from passing through the negatively charged cell

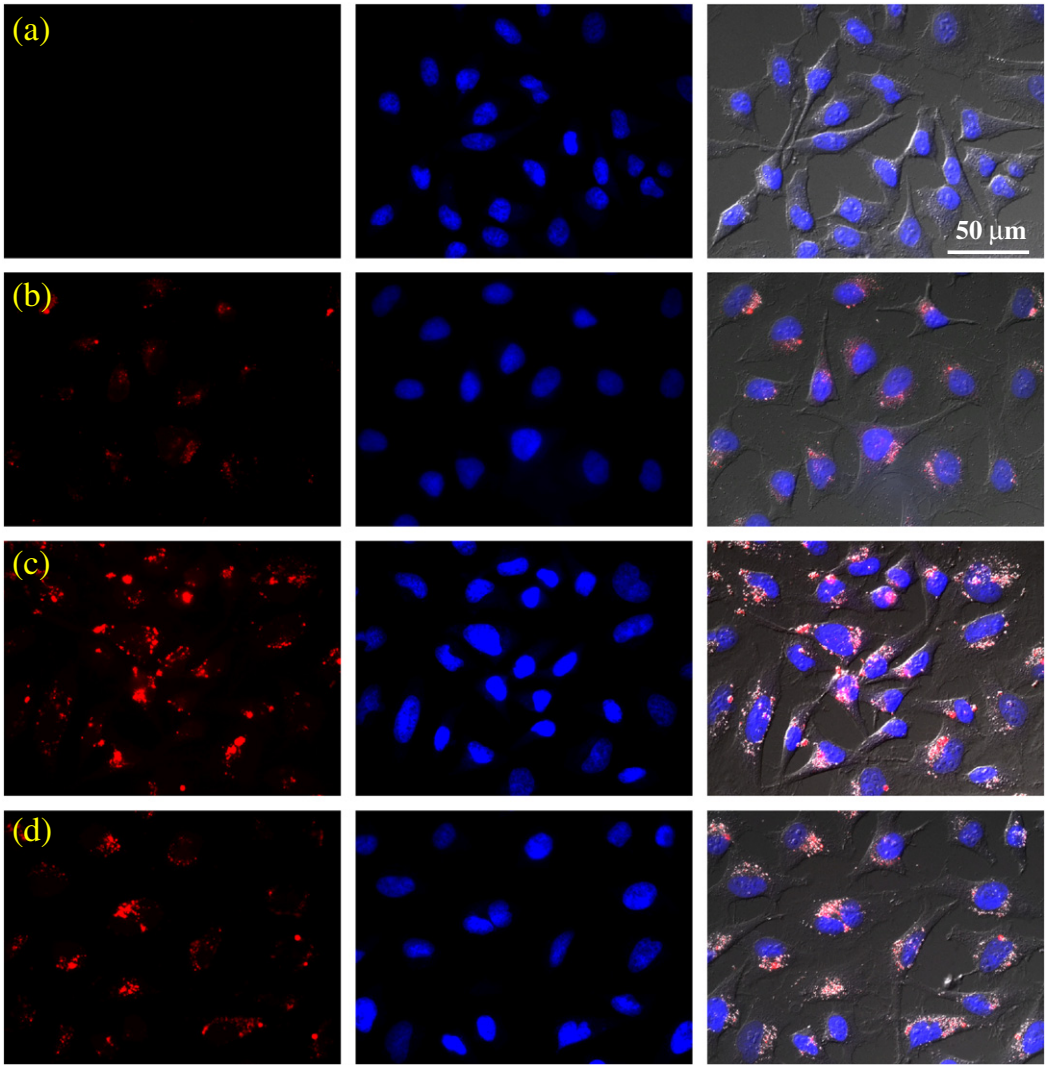

Fig. 1. Comparison of images of HeLa cells after 6 h incubation in DMEM containing FBS (10% unless otherwise specified) and (a) FND-COOH, (b) FND-COOH without 10% FBS, (c) FND-Tf, and (d) FND-NH_2 particles at a particle concentration of 10 μg mL^{-1}. The displayed images are epifluorescence images of FND particles (red) and stained nuclei (blue) (Hoechst 33342), and their overlap with the differential interference contrast (DIC) images of cells (first, second, and third columns).

membrane might be responsible for the negligible internalization. Alternatively, the observation of the fluorescence images of FND-COOH particles under a condition without serum in Fig. 1(b) is likely due to starving cells that consume indiscriminately. Several authors have reported the cellular uptake of FND-COOH particles in a serum-supplemented medium; this uptake, however, is highly ineffective compared to that without serum [11,12,53,54]. Our results are consistent with previous results except for the difference in internalization efficiency in a serum-supplemented medium. Several factors could have contributed to this discrepancy, including particle size, surface modification, and particle agglomeration, which could facilitate or block the uptake in a complex serum-supplemented medium. Nevertheless, the internalization of FND-COOH particles proceeds through an ineffective cellular uptake due largely to the repulsion of negative charges between the surface of the particles and the membrane of the cells.

The efficient internalization of FND-Tf and FND-NH_2 particles was observed in Fig. 1(c)–(d), showing a significant quantity of FND-Tf and FND-NH_2 particles internalized by cells, respectively. A comparison of Fig. 1(c)–(d) further reveals a lower degree of fluorescence intensity of FND-NH_2 particles, relative to that of FND-Tf particles. Internalization of nanoparticles by a cell generally involves two steps, the initial interaction between nanoparticle and cell surface, and the subsequent uptake of the nanoparticle by cellular endocytosis. The internalization of FND-Tf particles was confirmed through the cellular endocytosis triggered by receptor-mediated interactions — Tf-TfR interactions, with the support of a control experiment in which the fluorescence of FND-Tf particles was absent due to a blocking of the surface receptors of cells. Substantial fluorescence signals of FND-NH_2 particles are attributed to the cellular endocytosis triggered by surface electrostatic interactions between the negatively charged cell membrane and the positively charged amino groups on the surface of FND-NH_2, but the interaction through surface chemical group–amino groups was also plausible. These results indicate that the receptor-mediated endocytosis of FND-Tf particles was more effective than the cellular endocytosis of FND-NH_2 particles triggered by the interactions of surface charges and chemical groups.

3.2. Internalization efficiency and reaction time

To compare the efficiency with which FND-NH_2 and FND-Tf particles are internalized, the quantity of internalized particles was analyzed by flow cytometry. Fig. 2(a) shows the quantities of internalized FND-NH_2 and FND-Tf particles after 6 h incubation at particle concentrations in the region of 1–20 μg mL^{-1}, in which both internalized FND variants increased almost linearly but with different slopes prior to attaining their respective saturation values, both at a particle concentration of 10 μg mL^{-1}. The increased slope and nearly two-fold enhancement for FND-Tf particles, relative to FND-NH_2 particles at saturation levels, reflects two separate endocytic paths. The internalization of Tf conjugates and Tf-conjugated nanoparticles is well known to proceed through clathrin-mediated endocytosis, following Tf-TfR interactions [26–28]. The pathway for the cellular endocytosis of FND-NH_2 particles triggered by surface electrostatic and chemical interactions is unidentified previously, but our proposition of a different endocytic pathway is consistent with a previous report on the uptake of positively and negatively charged polystyrene nanoparticles by HeLa cells, in which the clathrin-dependent pathway plays a minor role for particle internalization

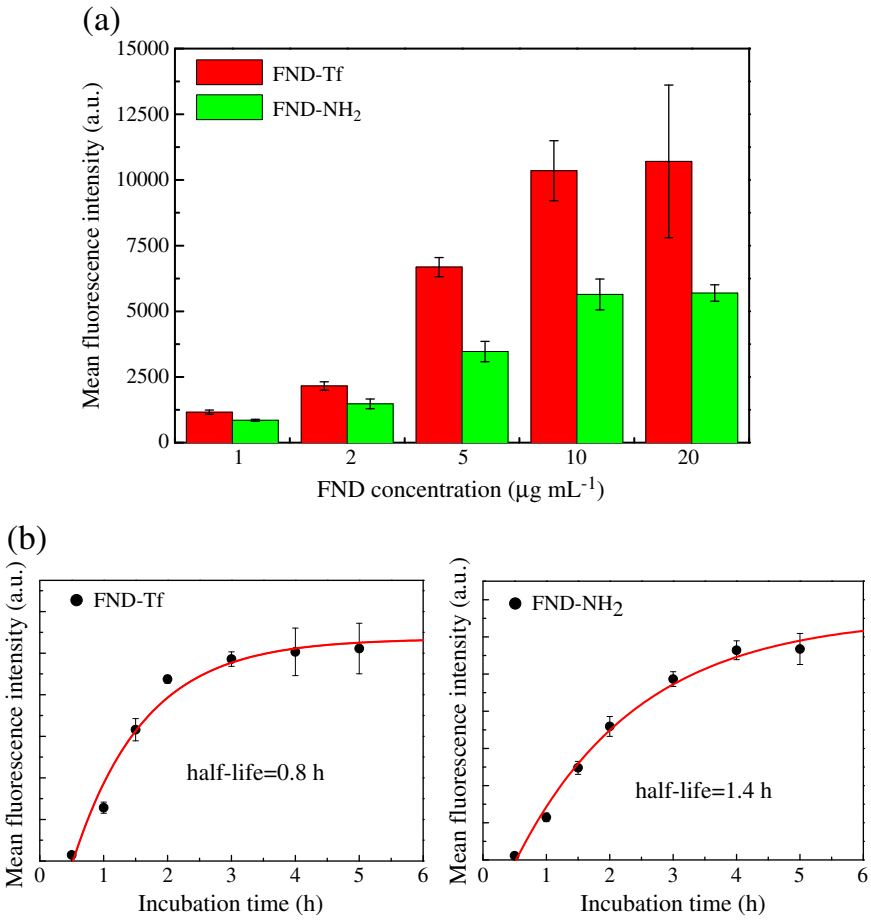

Fig. 2. Flow cytometry analysis of FND-Tf and FND-NH_2 particles internalized by a HeLa cell. (a) Comparison of the mean intensity of fluorescence as a function of particle concentration after 6 h incubation. (b) Reaction times at a particle concentration of 10 μg mL^{-1}.

[55]. Furthermore, the internalization of FND-NH_2 might proceed through the macropinocytosis dependent pathway, an important pathway for the internalization of positively charged polystyrene nanoparticles, because both nanoparticles have amino groups on the surface. In contrast to saturation, previous results have shown that the amounts of FND-FA (folic acid conjugated FND) and FND-Tf particles internalized by cells increase linearly with the particle concentration (1–100 μg mL^{-1}) [14,29]. This difference in internalization efficiency might be attributed to surface modification and facile agglomeration of the particles in medium.

For kinetic testing, reaction times were determined at 10 μg mL^{-1}. Fig. 2(b) shows the temporal profiles of internalized FND-NH_2 and FND-Tf particles; the solid curves indicate the data was fitted according to equation $I(t)=A[1-\exp(-k(t-t_c))]$, in which $I(t)$ is the mean intensity of fluorescence at a selected time, A is the saturation value of mean fluorescence intensity, k is the rate constant, and t_c is the lag in particle diffusion and targeting. Evidently, the uptake of FND-Tf particles increases more significantly and attains a greater saturation value in the third hour of incubation, with a half-life of ~0.8 h, whereas FND-NH_2 particles required longer to attain the saturation value, with a fourth hour of incubation and half-life of ~1.4 h. This increase in the rate of FND-Tf supports the proposition that FND-Tf and FND-NH_2 particles utilize two endocytic pathways, but the reduced rate of FND-NH_2 related to the removal of functional moieties before the cellular uptake cannot be excluded because the silanisation on the surface of particles might lead to products prone to hydrolysis under physiological conditions [56]. The half-life of ~0.8 h for FND-Tf was close to 0.7 h for FND-FA, indicating the internalization of particles through receptor-mediated endocytosis is nearly the same. The half-life of 1.3 h determined by Li and Zhou was high, reflecting an ineffective cellular uptake. The structural variation of transferrins on the surface of particles could have contributed to that, because the relative

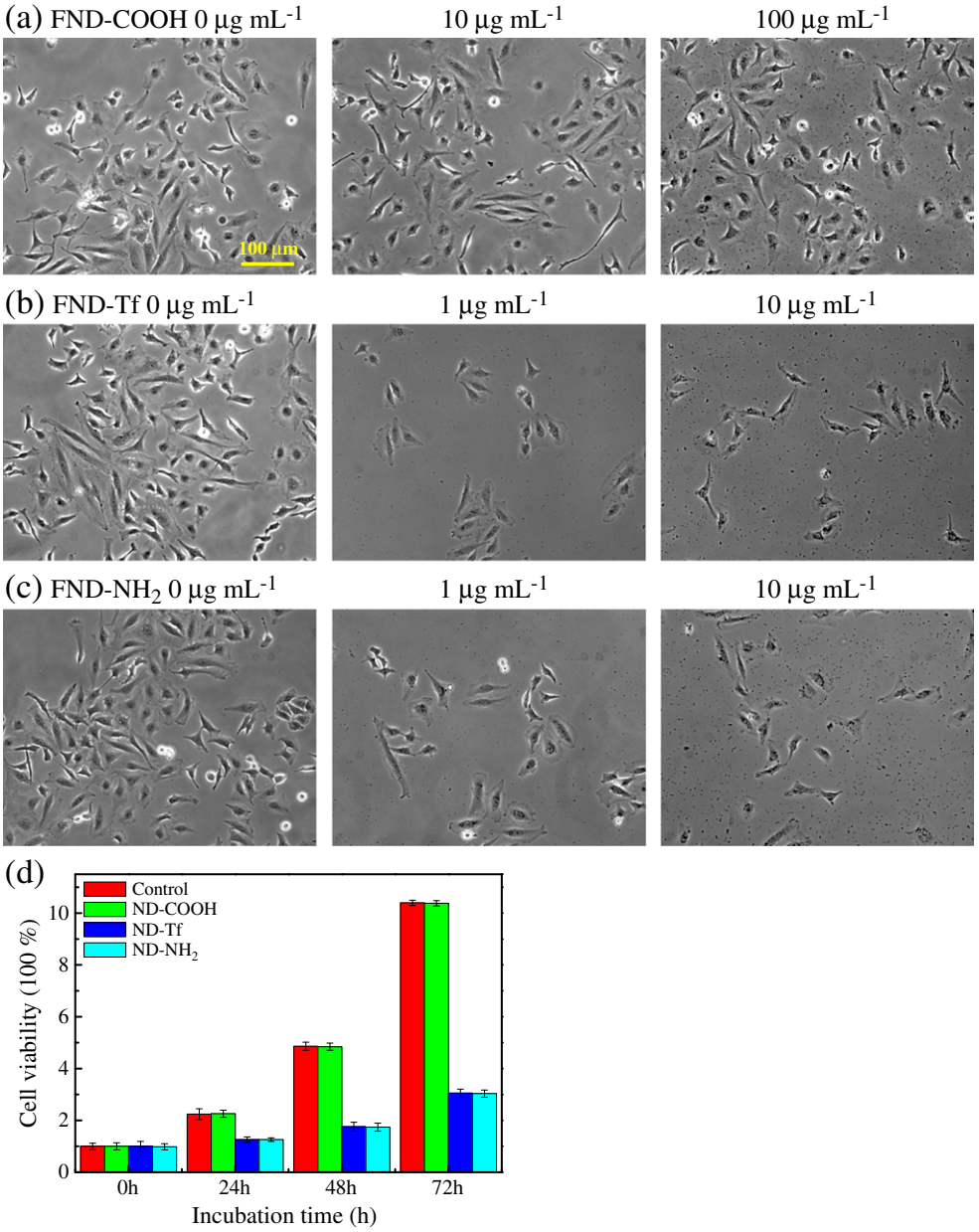

Fig. 3. Growth inhibition of HeLa cells incubated with FND-COOH, FND-Tf and FND-NH_2 particles. The bright-field images of cells recorded with a 10× objective after 48 h incubation with (a) FND-COOH at particle concentrations of 0, 10 and 100 μg mL^{-1}, and (b) FND-Tf and (c) FND-NH_2 at particle concentrations of 0, 1 and 10 μg mL^{-1}, respectively. (d) MTT assay of cell viability after 0, 24, 48 and 72 h incubation with ND-COOH, ND-Tf and ND-NH_2 particles at a particle concentration of 10 μg mL^{-1}, respectively.

charge of FND-Tf to FND-COOH particles was positive rather than negative, in contrast to the negative characteristics of free transferrins in medium and our zeta potential results.

3.3. Inhibition of cellular growth

The biocompatibility of nanoparticles is a key issue in biological applications, particularly regarding enduring cytotoxicity *in vivo*. Fig. 3(a) shows an indiscernible variation in the proliferation of cells following 48 h incubation with FND-COOH particles in a complete medium at particle concentrations of 0, 10 and 100 μg mL^{-1}, respectively. As revealed above, no FND-COOH particles were internalized by cells in a complete medium, indicating the negligible cytotoxicity of extracellular FND-COOH particles. In contrast, Fig. 3(b)–(c) shows a considerable inhibition of cellular growth after 48 h incubation with FND-NH_2 and FND-Tf particles at 1 and 10 μg mL^{-1}, respectively. The cytotoxicity was attributed to FNDs within the cells, rather than in the medium, according to the results from FND-COOH. The effective endocytic pathways of FND-Tf and FND-NH_2 particles also accounted for the high degree of cytotoxicity observed at low particle concentrations. To quantify the inhibition of growth, we evaluated cell viability using the MTT assay after incubation with ND-COOH, ND-Tf and ND-NH_2 at 10 μg mL^{-1}. We opted to use NDs rather than FNDs to avoid interference associated with the fluorescence of FND variants. The NDs were treated with thermal annealing and strong oxidizing acids under the same conditions to ensure the surface characteristics were the same as those of FNDs. As shown in Fig. 3(d), the rate of proliferation of treated cells, relative to untreated cells, decreased to >50% after 24 h incubation with ND-Tf or ND-NH_2 particles. A similar trend in the number of untreated and treated cells further supports the MTT results.

The large cytotoxicity of ND-Tf particles inside cells is attributed to the internalization through an effective pathway — receptor-mediated endocytosis. As for ND-NH_2 particles, the considerable cytotoxicity is in agreement with a previous report on 200-nm silica nanotubes (SNTs), which increased in toxicity due to their outer surfaces functionalized with amino groups through the silanisation with APTES molecules, and this toxicity was attributed to an increase in cellular uptake through surface electrostatic interactions [57]. Several studies have demonstrated that ND or FND particles of various sizes and different chemical surface functionality were nontoxic [9–14,19,50], but Faklaris et al. observed a ~20% decrease in cell viability after incubating <50 nm NDs for 48 h in 53 μg mL^{-1} [53]. Furthermore, Marcon et al. reported the cytotoxicity of 5 nm NDs functionalized with amine at ≥50 μg mL^{-1} and found the increase in toxicity correlated with the chemical surface functionality in the rank: $-NH_2 \gg -OH > -COOH$ [58]. The discrepancy in particle concentration is attributed to the difference in internalization efficiency, but the cytotoxicity observed in the literature is in agreement with ours in ND-NH_2 and ND-Tf particles.

3.4. Phototoxicity of internalized FND-Tf

Although inhibition was evident, the treated cells remained alive without a significantly altered morphology, enabling the evaluation of the phototoxicity of FND-Tf particles internalized by cells. We irradiated the cells (treated with FND-Tf particles at 1 μg mL^{-1}) through a 40× objective on a fluorescence microscope at wavelengths of 590–650 and 510–560 nm, respectively. The wavelengths (both with a power density of 7 W cm^{-2}), were selected using filters from a 100-W Hg lamp. Control experiments were performed under the same conditions. The untreated cells remained alive following exposure at both wavelengths for 2–3 h, and subsequent proliferation further confirmed cell viability. No death of the treated cell was observed after irradiation at 590–650 nm for 2 h; however, >90% of the treated cells were dead within 1 h following irradiation at 510–560 nm. Fig. 4 shows DIC images of treated and untreated cells under irradiation at 510–560 nm, in which the morphology of treated cells was significantly altered between 30–60 min. These results indicate that the death of treated cells was strongly associated with the absorption of isolated nitrogen atoms in FNDs at ≤550 nm, not N-V° nor N-V^- centers in 520–650 nm. The fact that the absorption of both N-V centers played only a minor role in killing was expected, as the absorption was efficiently converted into fluorescence at longer wavelengths, with a quantum yield close to the unit [59].

To kill the treated cells and evaluate the efficiency with which this was performed, we irradiated treated and untreated cells for 10 min with a CW laser at 532 nm. Following irradiation, we examined cell viability by adding calcein AM and EthD-1 to the medium. The green fluorescence of calcein AM and red fluorescence of EthD-1 indicated viable and dead cells, respectively [32]. Fig. 5 shows a time

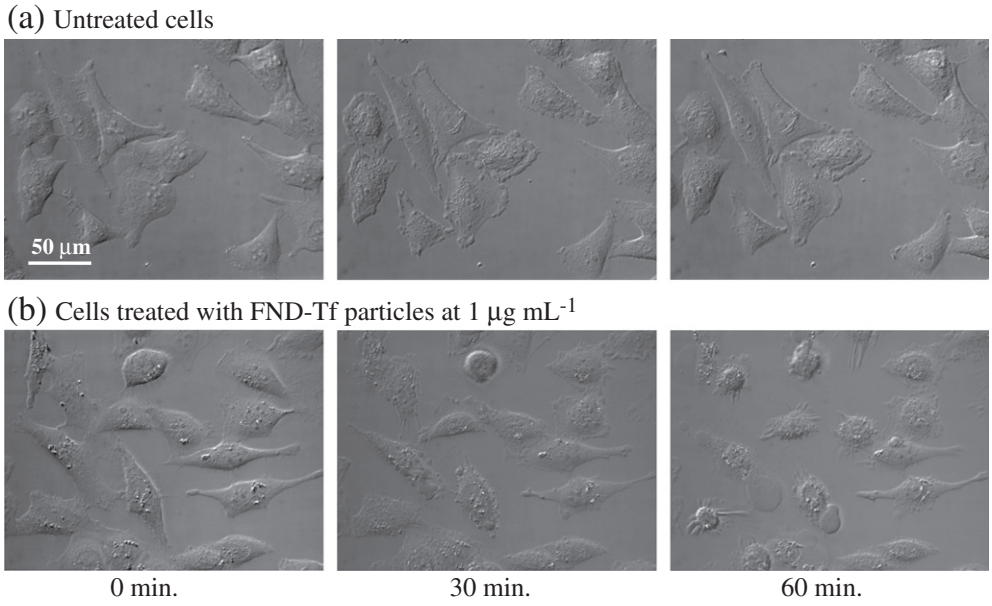

Fig. 4. Time series of the DIC images of (a) untreated and (b) treated cells with FND-Tf particles at 1 μg mL^{-1} for 6 h incubation, showing the enhanced photokilling of internalized FND-Tf particles. The images were recorded with a 40× objective under irradiation for 0, 30 and 60 min with 510–560 nm at a power density 7 W cm^{-2}, selected with a filter from a 100-W Hg lamp.

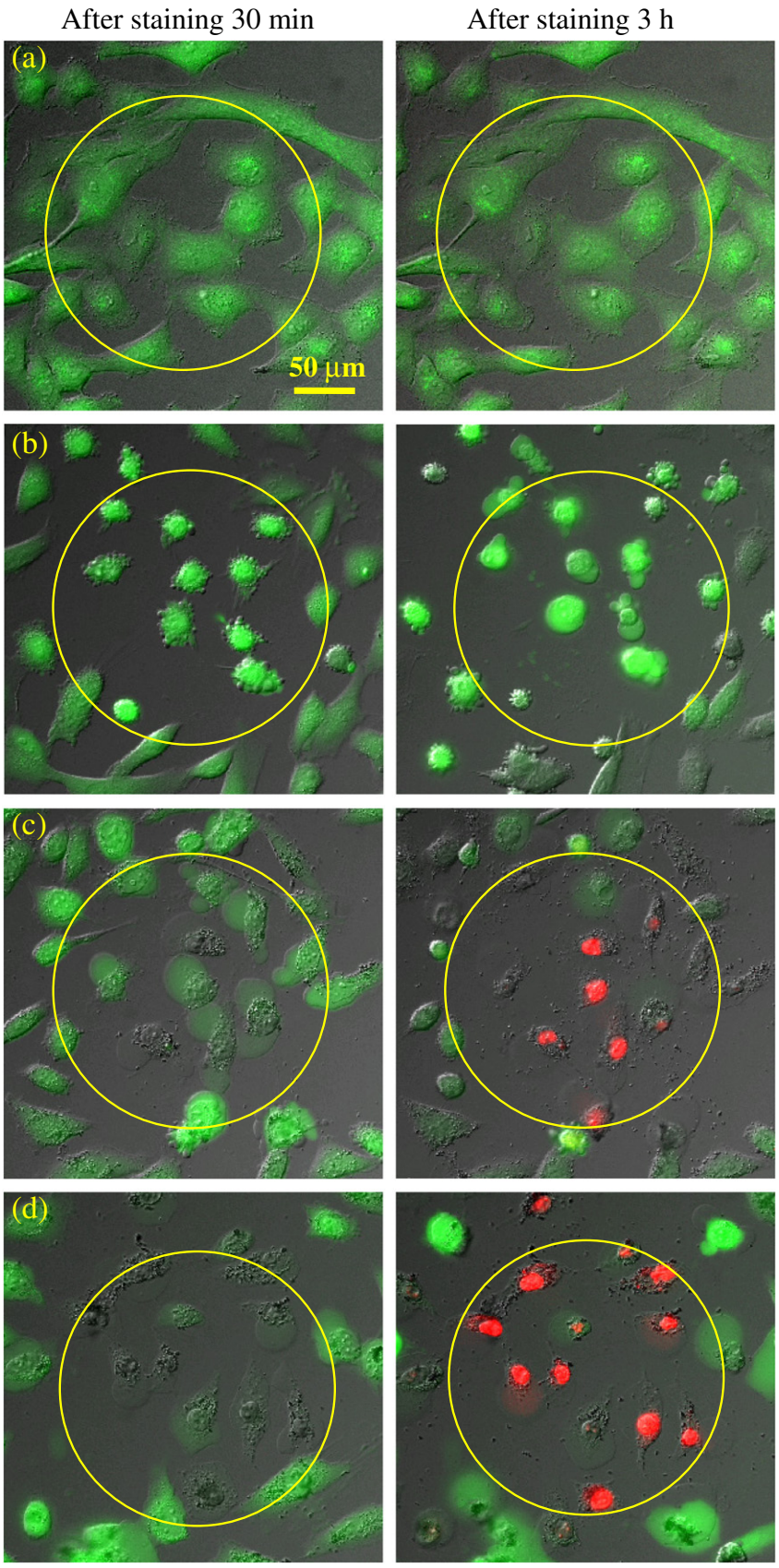

Fig. 5. DIC and fluorescence images of untreated cells after 10 min irradiation at 532 nm at power densities of (a) 50 and (b) 75 W cm^{-2}, and cells treated with FND-Tf particles at 10 μg mL^{-1} under the same irradiation conditions but at (c) 25 and (d) 50 W cm^{-2}. Fluorescence images of Calcein AM and EthD-1, added immediately after the irradiation to examine cell viability. The images of fluorescence in the cells were recorded after staining 30 min (left) and 3 h (right); a yellow circle indicates the region of laser irradiation.

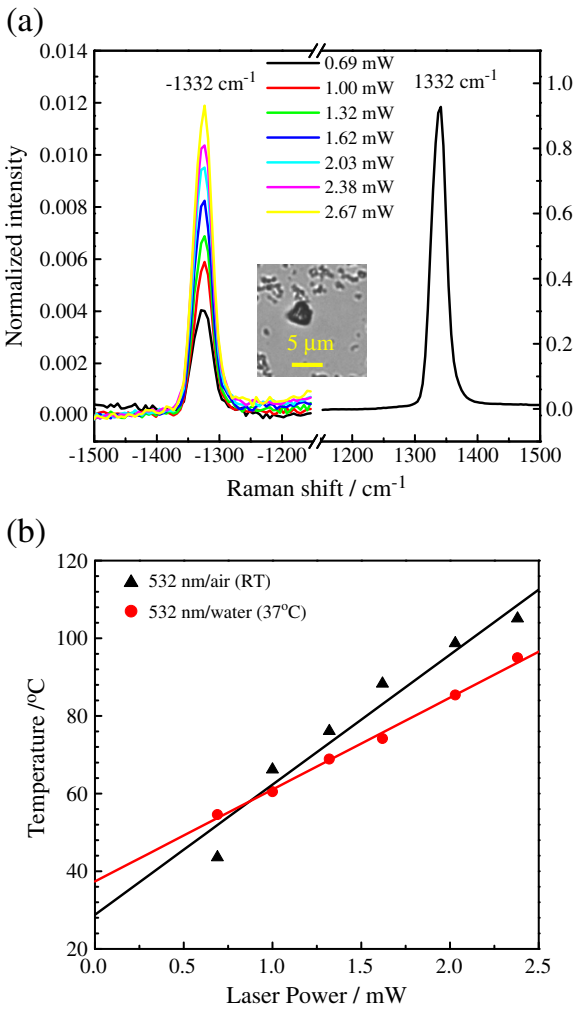

Fig. 6. Temperature elevation of a nanodiamond cluster under irradiation with a laser at 532 nm. (a) The increase in anti-Stokes Raman signals (at $-1332\ cm^{-1}$) of the ND cluster on a glass slide with laser energies at 0.69–2.67 mW; the Stokes signals at $1332\ cm^{-1}$ were set to the same for normalization. Insert: image of the ND cluster for measurements. (b) Temperature increase in the ND cluster as a function of laser energy under two conditions — in air (~29 °C) and in water within an incubator (37 °C); solid lines indicate the linear fit.

series of the overlay of fluorescence and DIC images of the treated and untreated cells after 10 min irradiation; the region of irradiation is marked with a yellow circle. As seen in the morphology in Fig. 5(a)–(b), the untreated cells remained alive even after 3 h staining and 10 min irradiation at $50\ W\ cm^{-2}$, but were killed at $75\ W\ cm^{-2}$. Because the dead cells retained green fluorescence after 3 h in Fig. 5(b), the death of cells was further confirmed from the lack of cell growth over 24 h and the delay in red fluorescence when the calcein AM/EthD-1 was added not immediately but after 12 h of the 10 min irradiation. This result indicated that the killing was not particularly violent, such that the dead cells required more time to deactivate the intracellular esterases. In contrast, Fig. 5(c)–(d) shows the evidently dead FND-treated cells after irradiation at 25 and $50\ W\ cm^{-2}$, respectively, with the support of cells bubbled showing red rather than green fluorescence. These results demonstrate that less than half the laser energy was required to kill the treated cells than for the untreated cells, and the severe destruction of the FND-treated cells caused a rapid deactivation of the intracellular esterases. The efficiency with which of FND-Tf particles are capable of photokilling is comparable to that of gold nanospheres with the maximum absorption at 520 nm, as reported previously [31]. Wavelengths ≤550 nm, compared to the strong absorption of gold-based nanomaterials of various forms in the near infrared (NIR) region, were inferior in penetration depth [33,60,61]. However, bioconjugated FND particles are relatively easy to prepare, biocompatible, and can be used as agents for both fluorescence imaging and photokilling.

The cell death likely resulted from a conversion of absorbed light into heat by FND particles. To provide a direct evidence of the temperature increase, we measured the anti-Stokes and Stokes Raman signals of a nanodiamond cluster upon 532 nm irradiation to calculate the temperature of the ND cluster. Fig. 6(a) illustrates an increase in the anti-Stokes Raman signals (at $-1332\ cm^{-1}$) of the C – C stretching vibration with an increase in laser energy; the Stokes Raman signal at $1332\ cm^{-1}$ of each spectrum was set to the same level [62]. From the intensity ratio of the anti-Stokes and Stokes Raman signals at each selected level of laser energy, we calculated the temperature according to the equation $I_{anti\text{-}stokes}/I_{stokes} = (\nu_l + \nu_{vib})^4 e^{-hc\nu_{vib}/kT}/(\nu_l - \nu_{vib})^4$, in which appear laser wavenumber ν_l, $\nu_{vib} = 1332\ cm^{-1}$, Boltzmann constant k and temperature T/K of the nanodiamond cluster. Fig. 6(b) shows the temperature increase in the nanodiamond cluster as a function of laser energy in air (~29 °C) and in water within an incubator (37 °C). The laser energy appears to have been converted into heat energy and the temperature increased more rapidly in air. We have tried to measure the weak anti-Stokes Raman signals of the ND-Tf particles inside a cell; however, strong scattering from cell components prevented this measurement.

4. Conclusion

We investigated the quantity and reaction time of FND-Tf and FND-NH_2 particles internalized by HeLa cells to gain a more complete understanding of endocytic processes through receptor mediation and surface electrostatic interactions. We observed that the cellular uptake of FND-Tf and FND-NH_2 particles reached different saturation values, with half-life times of 0.8 and 1.4 h, respectively. The increase in saturation value and decrease in half-life of FND-Tf particles indicate that the receptor-mediated endocytosis was nearly twice as effective. Furthermore, we observed a significant inhibition in cellular growth, with a proliferation rate decreasing to >50% after 24 h at a particle concentration one tenth that previously reported for surface-unmodified FND particles. The enhanced killing of cells following irradiation of internalized FND-Tf at 532 nm was observed and confirmed through the photothermal effect from Raman signals of the C – C stretching vibration of nanodiamonds. The high uptake efficiency of FND-Tf particles through receptor-mediated endocytosis, together with reported cytotoxicity and phototoxicity, pave the way for the use of FND-Tf particles in effectively targeted imaging and the enhanced photokilling of cancer cells.

Acknowledgments

National Synchrotron Radiation Research Center (NSRRC) and National Science Council (NSC 96-2113-M-213-005-MY2 and NSC 99-2113-M-213-005-MY2) in Taiwan provided financial support. We thank Dr. Huan-Cheng Chang at IAMS for the use of the flow cytometry and Prof. Lih-Yuan Lin in NTHU and Dr. Cheng-Chin Kuo at NHRI for their valuable suggestions on inhibition of cell growth and phototoxicity assay.

References

[1] N. Sanvicens, M.P. Marco, Trends Biotechnol. 26 (2008) 425.
[2] K.C. Weng, C.O. Noble, B. Papahadjopoulos-Sternberg, F.F. Chen, D.C. Drummond, D.B. Kirpotin, D. Wang, Y.K. Hom, B. Hann, J.W. Park, Nano Lett. 8 (2008) 2851.
[3] A.H. Lu, E.L. Salabas, F. Schüth, Angew. Chem. Int. Ed. 46 (2007) 1222.
[4] L. Duchesne, D. Gentili, M. Comes-Franchini, D.G. Fernig, Langmuir 24 (2008) 13572.
[5] X. Michalet, F.F. Pinaud, L.A. Bentolila, J.M. Tsay, S. Doose, J.J. Li, G. Sundaresan, A.M. Wu, S.S. Gambhir, S. Weiss, Science 307 (2005) 538.

[6] M. Ferrari, Nat. Rev. Cancer 5 (2005) 161.
[7] A.M. Schrand, L. Dai, J.J. Schlager, S.M. Hussain, E. Osawa, Diamond Relat. Mater. 16 (2007) 2118.
[8] A. Krueger, Chem. Eur. J. 14 (2008) 1382.
[9] K.K. Liu, C.L. Cheng, C.C. Chang, J.I. Chao, Nanotechnology 18 (2007) 325102.
[10] V. Vaijayanthimala, H.C. Chang, Nanomedicine 4 (2009) 47.
[11] S.J. Yu, M.W. Kang, H.C. Chang, K.M. Chen, Y.C. Yu, J. Am. Chem. Soc. 127 (2005) 17604.
[12] C.C. Fu, H.Y. Lee, K. Chen, T.S. Lim, H.Y. Wu, P.K. Lin, P.K. Wei, P.H. Tsao, H.C. Chang, W. Fann, Proc. Natl. Acad. Sci. U. S. A. 104 (2007) 727.
[13] Y.R. Chang, H.Y. Lee, K. Chen, C.C. Chang, D.S. Tsai, C.C. Fu, T.S. Lim, Y.K. Tzeng, C.Y. Fang, C.C. Han, H.C. Chang, W. Fann, Nat. Nanotechnol. 3 (2008) 284.
[14] B. Zhang, Y. Li, C.Y. Fang, C.C. Chang, C.S. Chen, Y.Y. Chen, H.C. Chang, Small 5 (2009) 2716.
[15] M.F. Weng, S.Y. Chiang, N.S. Wang, H. Niu, Diam. Relat. Mater. 18 (2009) 587.
[16] A. Kruger, Y. Liang, G. Jarre, J. Stegk, J. Mater. Chem. 16 (2006) 2322.
[17] C.Y. Cheng, E. Perevedentseva, J.S. Tu, P.H. Chung, C.L. Cheng, K.K. Liu, J.I. Chao, P.H. Chen, C.C. Chang, Appl. Phys. Lett. 90 (2007) 163903.
[18] O. Faklaris, V. Joshi, T. Irinopoulou, P. Tauc, M. Sennour, H. Girard, C. Gesset, J.C. Arnault, A. Thorel, J.P. Boudou, P.A. Curmi, F. Treussart, ACS Nano 3 (2009) 3955.
[19] V. Vaijayanthimala, Y.K. Tzeng, H.C. Chang, C.L. Li, Nanotechnology 20 (2009) 425103.
[20] M. Mkandawire, A. Pohl, T. Gubarevich, V. Lapina, D. Appelhans, G. Rodel, W. Pompe, J. Schreiber, J. Optiz, J. Biophotonics 2 (2009) 596.
[21] F. Neugart, A. Zappe, F. Jelezko, C. Tietz, J.P. Boudou, A. Krueger, J. Wrachtrup, Nano Lett. 7 (2007) 3588.
[22] Y.Y. Hui, B. Zhang, Y.C. Chang, C.C. Chang, H.C. Chang, J.H. Hsu, K. Chang, F.H. Chang, Opt. Express 18 (2010) 5896.
[23] N. Yamamoto, F. Fukai, H. Ohshima, H. Terada, K. Makino, Colloids Surf. B 25 (2002) 157.
[24] S.J. Tan, N.R. Jana, S. Gao, P.K. Patra, J.Y. Ying, Chem. Mater. 22 (2010) 2239.
[25] M. Das, D. Mishra, T.K. Maiti, A. Basak, P. Pramanik, Nanotechnology 19 (2008) 415101.
[26] T.R. Daniels, T. Delgado, J.A. Rodriguez, G. Helguera, M.L. Penichet, Clin. Immunol. 121 (2006) 144.
[27] S.A. Mousavi, L. Malerod, T. Berg, R. Kjeken, Biochem. J. 377 (2004) 1.
[28] K.T. Yong, J. Qian, I. Roy, H.H. Lee, E.J. Bergey, K.M. Tramposch, S. He, M.T. Swihart, A. Maitra, P.N. Prasad, Nano Lett. 7 (2007) 761.
[29] Y.Q. Li, X.P. Zhou, Diam. Relat. Mater. 19 (2010) 1163.
[30] M. Stobiecka, M. Hepel, Biomaterials 32 (2011) 3312.
[31] I.H. El-Sayed, X. Huang, M.A. El-Sayed, Cancer Lett. 239 (2006) 129.
[32] F.Y. Cheng, C.T. Chen, C.S. Yeh, Nanotechnology 20 (2009) 425104.
[33] X. Huang, I.H. El-Sayed, W. Qian, M.A. El-Sayed, J. Am. Chem. Soc. 128 (2006) 2115.
[34] S. Ghosh, S. Dutta, E. Gomes, D. Carroll, R. D'Agostino Jr., J. Olson, M. Guthold, W.H. Gmeiner, ACS Nano 3 (2009) 2667.
[35] A. Bruke, X. Ding, R. Singh, R.A. Kraft, N. Levi-Polyachenko, M.N. Rylander, C. Szot, C. Buchanan, J. Whitney, J. Fisher, H.C. Hatcher, R. D'Agostino Jr., N.D. Kock, P.M. Ajayan, D.L. Carroll, S. Akman, F.M. Torti, S.V. Torti, Proc. Natl. Acad. Sci. U. S. A. 106 (2009) 12897.
[36] R.R. Anderson, J.A. Parrish, Science 220 (1983) 524.
[37] N.J. Durr, T. Larson, D.K. Smith, B.A. Korgel, K. Sokolov, A. Ben-Yakar, Nano Lett. 7 (2007) 941.
[38] D. Gao, R.R. Agayan, H. Xu, M.A. Philbert, R. Kopelman, Nano Lett. 6 (2006) 2383.
[39] D. Pissuwan, S.M. Valenzuela, C.M. Miller, M.B. Cortie, Nano Lett. 7 (2007) 3808.
[40] X. Huang, P.K. Jain, I.H. El-Sayed, M.A. El-Sayed, Nanomedicine 2 (2007) 681.
[41] R.S. Norman, J.W. Stone, A. Gole, C.J. Murphy, T.L. Sabo-Attwood, Nano Lett. 8 (2008) 302.
[42] S.V. Torti, F. Byrne, O. Whelan, N. Levi, B. Ucer, M. Schmid, F.M. Torti, S. Akman, J. Liu, P.M. Ajayan, O. Nalamasu, D.L. Carroll, Int. J. Nanomedicine 2 (2007) 707.
[43] N.W. Kam, M. O'Connell, J.A. Wisdom, H. Dai, Proc. Natl. Acad. Sci. U. S. A. 102 (2005) 11600.
[44] P. Chakravarty, R. Marches, N.S. Zimmerman, A.D.E. Swafford, P. Bajaj, I.H. Musselman, P. Pantano, R.K. Draper, E.S. Vitetta, Proc. Natl. Acad. Sci. U. S. A. 105 (2008) 8697.
[45] T.L. Wee, Y.K. Tzeng, C.C. Huan, H.C. Chang, W. Fann, J.H. Hsu, K.M. Chen, Y.C. Yu, J. Phys. Chem. A 111 (2007) 9379.
[46] M.L. Schipper, G.I.A.L. Koh, Z. Cheng, Y. Ebenstein, A. Aharoni, S. Keren, L.A. Bentolila, J. Li, J. Rao, X. Chen, U. Banin, A.M. Wu, R. Sinclair, S. Weiss, S.S. Gambhir, Small 5 (2009) 126.
[47] C.C. Chang, P.H. Chen, H.L. Chu, T.C. Lee, C.C. Chou, J.I. Chao, S.Y. Su, J.S. Chen, J.S. Tsai, C.M. Tsai, Y.P. Ho, K.W. Sun, C.L. Cheng, F.R. Chen, Appl. Phys. Lett. 93 (2008) 033905.
[48] X.L. Kong, L.C.L. Huang, C.M. Hsu, W.H. Chen, C.C. Han, H.C. Chang, Anal. Chem. 77 (2005) 259.
[49] R.P. Bagwe, L.R. Hilliard, W. Tan, Langmuir 22 (2006) 4357.
[50] S. Vial, C. Mansuy, S. Sagan, T. Irinopoulou, F. Burlina, J.-P. Boudou, G. Chassaing, S. Lavielle, Chembiochem 9 (2008) 2113.
[51] H. Cao, J. He, L. Deng, X. Gao, Appl. Surf. Sci. 255 (2009) 7974.
[52] Y.Y. Hui, C.L. Cheng, H.C. Chang, J. Phys. D: Appl. Phys. 43 (2010) 374021.
[53] O. Faklaris, D. Garrot, V. Joshi, F. Druon, J.P. Boudou, T. Sauvage, P. Georges, P.A. Curmi, F. Treussart, Small 4 (2008) 2236.
[54] K.K. Liu, M.F. Chen, P.Y. Chen, T.J.F. Lee, C.L. Cheng, C.C. Chang, Y.P. Ho, J.I. Chao, Nanotechnology 19 (2008) 205102.
[55] J. Dausend, A. Musyanovych, M. Dass, P. Walther, H. Schrezenmeier, K. Landfester, V. Mailander, Macromol. Biosci. 8 (2008) 1135.
[56] M.C.B. Salon, M. Abdelmouleh, S. Boufi, M.N. Belgacem, A. Gandini, J. Colloid Interface Sci. 289 (2005) 249.
[57] A. Nan, X. Bai, S.J. Son, S.B. Lee, H. Ghandehari, Nano Lett. 8 (2008) 2150.
[58] L. Marcon, F. Riquet, D. Vicogne, S. Szunerits, J.F. Bodart, R. Boukherroub, J. Mater. Chem. 20 (2010) 8064.
[59] G. Davies, Properties and Growth of Diamond, EMIS Data Review Series No. 9, INSPEC, The Institution of Electrical Engineers, London, 1994.
[60] C. Loo, A. Lin, L. Hirsch, M.H. Lee, J. Barton, N. Halas, J. West, R. Drezek, Technol. Cancer Res. Treat. 3 (2004) 33.
[61] M. Hu, H. Petrova, J. Chen, J.M. McLellan, A.R. Siekkinen, M. Marquez, X. Li, Y. Xia, G.V. Hartland, J. Phys. Chem. B 110 (2006) 1520.
[62] E. Perevedentseva, P.-H. Chung, C.-L. Cheng, J. Vac. Sci. Technol. B 23 (2005) 1980.